

# A path to poor coherence in heavy fermions from Mott physics and hybridization

A. Amaricci<sup>1</sup>, L. de' Medici<sup>2</sup>, G. Sordi<sup>3</sup>, M.J. Rozenberg<sup>2,4</sup>, M. Capone<sup>1,5</sup>

<sup>1</sup> CNR-IOM, SISSA, Via Bonomea 265, 34136 Trieste, Italy.

<sup>2</sup> Laboratoire de Physique des Solides, CNRS-UMR8502, Université Paris-Sud, Orsay 91405, France.

<sup>3</sup> Theory Group, Institut Laue Langevin, 6 Rue J. Horowitz, 38042 Grenoble, France.

<sup>4</sup> Departamento de Física, FCEN, Universidad de Buenos Aires, Ciudad Universitaria Pab.I, Buenos Aires 1428, Argentina. and

<sup>5</sup> Physics Department, University "Sapienza", Piazzale A. Moro 2, 00185 Rome, Italy.

(Dated: November 17, 2018)

We investigate the anomalous metal arising by hole doping the Mott insulating state of the periodic Anderson model. Using Dynamical Mean-Field Theory we show that, as opposed to the electron-doped case, in the hole-doped regime the hybridization between localized and delocalized orbitals leads to the formation of composite quasi-particles reminiscent of the Zhang-Rice singlets. We compute the coherence temperature of this state, showing its extremely small value at low doping. As a consequence the weakly-doped Mott state deviates from the predictions of Fermi-liquid theory already at small temperatures. The onset of the Zhang-Rice state and of the consequent poor coherence is due to the electronic structure in which both localized and itinerant carriers have to be involved in the formation of the conduction states and to the proximity to the Mott state. By investigating the magnetic properties of this state, we discuss the relation between the anomalous metallic properties and the behavior of the magnetic degrees of freedom.

PACS numbers:

## I. INTRODUCTION

The rise of the field of strongly correlated materials revealed a number of unexpected intriguing phenomena which can not be explained within the standard theory of solids.<sup>1</sup> The paradigm of correlation effects is based on the Mott insulating state and the Mott-Hubbard metal-insulator transition,<sup>2,3</sup> but a key role is also played by high-temperature superconductivity in copper oxides<sup>4,5</sup> and the unconventional superconductivity at the edge of a magnetic phase observed in heavy fermions.<sup>6,7</sup> More recently, the partnership between exotic superconductivity, strong correlations and magnetism has been strengthened by the discoveries in the iron-based superconductors,<sup>8</sup> in the alkali-doped fullerenes<sup>9,10</sup> and possibly also in the molecular conductors based on aromatic molecules.<sup>11–13</sup>

A common companion of Mott physics and anomalous superconductivity is the deviation from the standard Fermi-Liquid (FL) theory in the metallic phase, or non-Fermi-liquid (NFL) behavior.<sup>14</sup> The FL theory describes a system of interacting fermions as a collection of renormalized non-interacting *quasi-particles* which propagate coherently in the solid.<sup>15</sup> The main qualitative effect of the electron-electron correlations is to enhance the effective mass and accordingly reduce the coherence of the Fermi gas. This reflects in a reduction of the coherence temperature, the scale at which the thermal fluctuations destroy the coherent motion. However in many compounds, most notably heavy fermion materials and underdoped cuprates, this picture breaks down and the carriers can no longer be described as long-lived excitations as they acquire a finite lifetime. This behavior directly influences the transport properties leading to anomalies in the temperature dependence of the resistivity.

In this paper we present a general mechanism based

on Mott physics and multi-band effects which leads to a metallic state with an extremely small FL coherence temperature. Empirically, this system will display a NFL behavior already at exceedingly small temperatures. The key element is the hybridization between a strongly correlated band and a weakly interacting band that leads to the formation of hybrid entities. The binding with the localized *f*-electrons hinders the motion of the carriers leading to a coherence temperature which is much smaller than the (already renormalized) scale predicted by FL theory on the basis of mass renormalization.

Our approach is based on the periodic Anderson model (PAM), a widely accepted correlated electrons model for the description of the heavy fermion physics. In its minimal form the PAM describes a set of non-dispersive strongly correlated electrons, hybridizing with a band of conduction electrons. In a general framework the PAM provides a more detailed description of the electronic configuration of correlated materials with respect to the Hubbard model, by taking into account the effects of the inclusion of non-correlated bands. We solved the PAM using dynamical mean-field theory (DMFT),<sup>16</sup> one of the most powerful and reliable tools to study correlated materials.

Following previous studies<sup>17–19</sup> we investigate the model around the Mott insulating state which takes place for large interactions and *odd* integer total occupation. The doping-driven transition has been thoroughly investigated in Ref. 17,19, and a NFL behavior in the hole-doped side has been demonstrated in Ref. 18. Here we extend this work by analyzing the coherence-incoherence crossover which leads to the NFL behavior and its dependence on doping. We will therefore focus on the scattering properties of the system and we will detail their relation with the magnetic degrees of freedom. Finally

we establish a connection between the finite-temperature breakdown of the FL and the competition between anti-ferromagnetic and ferromagnetic short-ranged correlations.

The manuscript is structured as follows. In Sec. II we introduce the PAM and the related DMFT equations. In section Sec. III we briefly discuss the doping-driven Mott transition in the PAM. In Sec. IV we present the main results of this work, namely the strongly incoherent nature of the low temperature metallic state. A phase-diagram of the model is presented at the end of this section. In Sec. V we study the magnetic properties of the model. Finally, we present a magnetic phase-diagram of the model which illustrates how magnetic competition helps stabilizing the incoherent behavior at low temperature.

## II. MODEL AND THEORETICAL FRAMEWORK

### A. The Periodic Anderson Model

The periodic Anderson model describes a set of non-dispersive strongly correlated electrons, locally hybridizing with a band of conduction electrons. The model Hamiltonian is written in the following form:

$$\begin{aligned} H &= H_0 + H_{fp} + H_I \\ H_0 &= - \sum_{\langle ij \rangle > \sigma} t_{ij} p_{i\sigma}^\dagger p_{j\sigma} + \epsilon_p \sum_{i\sigma} n_{pi\sigma} + \epsilon_f \sum_{i\sigma} n_{fi\sigma} \\ H_{fp} &= V_{fp} \sum_{i\sigma} (f_{i\sigma}^\dagger p_{i\sigma} + p_{i\sigma}^\dagger f_{i\sigma}) \\ H_I &= U \sum_i (n_{fi\uparrow} - \frac{1}{2}) (n_{fi\downarrow} - \frac{1}{2}) \end{aligned} \quad (1)$$

The operators  $p_{i\sigma}$  ( $p_{i\sigma}^\dagger$ ) destroy (create) conduction band electrons with hopping amplitude  $t_{ij}$  and energy  $\epsilon_p$ . The operators  $f_{i\sigma}$  ( $f_{i\sigma}^\dagger$ ) destroy (create) electrons in the non-dispersive orbital with energy  $\epsilon_f$ . The terms proportional to  $V_{fp}$  describe the hybridization between the two species. The interaction term  $H_I$  describes the strong on-site Coulomb repulsion experienced by  $f$ -orbital electrons.

The non-interacting lattice Green's function reads:

$$\hat{G}_{0\sigma}^{-1}(\mathbf{k}, i\omega_n) = \begin{pmatrix} i\omega_n + \mu - \epsilon_f & -V_{fp} \\ -V_{fp} & i\omega_n + \mu - \epsilon_p - \epsilon(\mathbf{k}) \end{pmatrix}$$

with  $\epsilon(\mathbf{k})$  the dispersion of the conduction electrons:  $\epsilon(\mathbf{k}) = \sum_{\langle ij \rangle} e^{-i\mathbf{k} \cdot (\mathbf{r}_i - \mathbf{r}_j)} t_{ij}$ . The corresponding interacting Green's function can be expressed by means of the following matrix Dyson equation:

$$\hat{G}_\sigma(\mathbf{k}, i\omega_n)^{-1} = \hat{G}_{0\sigma}^{-1}(\mathbf{k}, i\omega_n) - \hat{\Sigma}_\sigma(\mathbf{k}, i\omega_n) \quad (2)$$

where

$$\hat{\Sigma}_\sigma(\mathbf{k}, i\omega_n) = \begin{pmatrix} \Sigma_{f\sigma}(\mathbf{k}, i\omega_n) & 0 \\ 0 & 0 \end{pmatrix} \quad (3)$$

is the self-energy matrix  $\hat{\Sigma}_\sigma$ . The non-interacting nature of the conduction band is reflected in the existence of only one non-zero self-energy for the  $f$ -electrons. Nevertheless, it is useful to define an *effective* self-energy also for the conduction electrons as:

$$\Sigma_{p\sigma}(\mathbf{k}, i\omega_n) = \frac{V_{fp}^2}{i\omega_n + \mu - \epsilon_f - \Sigma_{f\sigma}(\mathbf{k}, i\omega_n)} \quad (4)$$

This function describes the dressing of the  $p$ -electrons as an effect of both their hybridization with the correlated  $f$ -electrons and, indirectly, of the Hubbard repulsion on the latter. In particular, the appearance of a finite imaginary part in the zero-frequency limit signals the breakdown of a FL picture for the conduction electrons.

Since  $\Sigma_{p\sigma}$  arises due to both the hybridization and the interaction  $U$ , it is not expected to vanish in the non-interacting limit  $U = 0$ . On the other hand, it is easy to realize that in this limit the pure hybridization can not lead to a finite imaginary part of  $\Sigma_{p\sigma}$  at zero frequency, and that any breakdown of the FL behavior can descend only from correlation effects.

### B. DMFT equations

The PAM has been studied using a large variety of numerical<sup>20–24</sup> and analytical methods.<sup>25–28</sup> To access the non-perturbative regime of the PAM, we investigate the solution of the model using the DMFT, which has been used to solve this model since its early stages.<sup>29,30</sup>

Within DMFT a lattice model is mapped onto an effective single-impurity problem, fixed by a self-consistency condition which enforces the equivalence between the two models as far as the local physics is concerned.<sup>16,31</sup> The scheme is equivalent to a local approximation on the self-energy, which becomes momentum independent.

The DMFT equations can be obtained using a quantum cavity method. The effective action of the single  $f$ -orbital impurity problem is obtained integrating out all lattice degrees of freedom except for a chosen site (labeled conventionally as site  $i = 0$ ) and keeping only the first term in the expansion<sup>16,32</sup> in terms of many-particle Green's functions:

$$\begin{aligned} S_{\text{eff}} &= - \int_0^\beta d\tau \int_0^\beta d\tau' \sum_\sigma f_{0\sigma}^+(\tau) \mathcal{G}_{0\sigma}^{-1}(\tau - \tau') f_{0\sigma}(\tau') \\ &+ U \int_0^\beta d\tau [n_{f0\uparrow}(\tau) - 1/2] [n_{f0\downarrow}(\tau) - 1/2] \end{aligned} \quad (5)$$

The action  $S_{\text{eff}}$  is expressed in terms of the local *Weiss Field*  $\mathcal{G}_{0\sigma}^{-1}(i\omega_n)$ , describing the quantum fluctuations at the correlated  $f$ -orbital. The Weiss field satisfies a self-consistence equation which depends on the lattice under consideration. In this work we consider a Bethe lattice with semi-elliptical density of states of half-bandwidth  $D$  (fixing the energy unit of the problem),

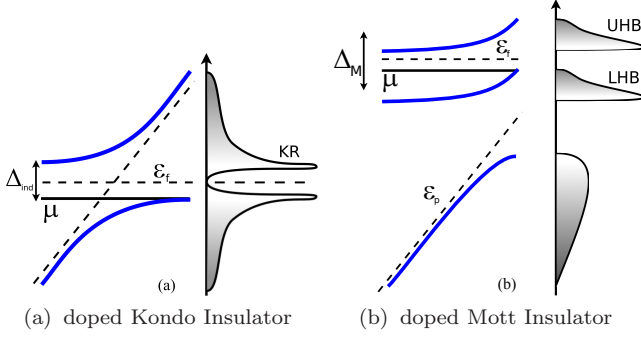


Figure 1: (Color online) Schematic representation of the doped Kondo (a) and doped Mott (b) insulators, inspired by Ref. 33. A schematic picture of the band structure is reported in the left side of each figure. The hybridized bands are indicated with thick (blue online) lines, dashed lines are used for the bare bands ( $V_{fp} = U = 0$ ). In the right sides we sketched the corresponding density of states. A lighter color indicates the more correlated character of the hybridized bands.

$D(\varepsilon) = \frac{2}{\pi D^2} \sqrt{D^2 - \varepsilon^2}$ . In this case the self-consistency is particularly simple and reads:

$$\mathcal{G}_{0\sigma}^{-1}(i\omega_n) = i\omega_n + \mu - \epsilon_f - \frac{V_{fp}^2}{i\omega_n + \mu - \epsilon_p - \frac{D^2}{4}G_{p\sigma}(i\omega_n)} \quad (6)$$

where  $G_{p\sigma}$  is the conduction electron local Green's function. The functional form of  $\mathcal{G}_{0\sigma}^{-1}$  mirrors in the DMFT equations the relation between the two orbitals in the lattice problem. The fluctuations at the  $f$ -orbital are in fact composed of two contributions: (a) the on-site quantum fluctuations and (b) indirect delocalization through conduction band proportional to squared hybridization amplitude.

The DMFT solution requires therefore to compute the impurity Green's function

$$G^{\text{imp}}(i\omega_n) = -i\langle f f^+ \rangle_{\text{S}_{\text{eff}}} \quad (7)$$

where the symbol  $\langle \rangle_{\text{S}_{\text{eff}}}$  indicates the average with respect to the effective action (5). From the knowledge of the impurity Green's function it is straightforward to determine the self-energy:

$$\Sigma(i\omega_n)_\sigma = \Sigma_\sigma^{\text{imp}}(i\omega_n) = \mathcal{G}_{0\sigma}^{-1}(i\omega_n) - G_\sigma^{\text{imp}^{-1}}(i\omega_n)$$

and finally to evaluate the local Green's function:

$$G_{p\sigma}(i\omega_n) = \int d\varepsilon \frac{D(\varepsilon)}{i\omega_n + \mu - \epsilon_p - \Sigma_{p\sigma}(i\omega_n) - \varepsilon}$$

Then a new Weiss field can be computed and the procedure can be iterated until convergence is achieved.

The solution of the effective impurity problem, *i.e.* Eq. (7), is the bottleneck of the DMFT algorithm. In this work we use a combination of numerical techniques:<sup>16</sup> Hirsch-Fye Quantum Monte Carlo (QMC)<sup>34,35</sup> and Exact Diagonalization (ED) methods,

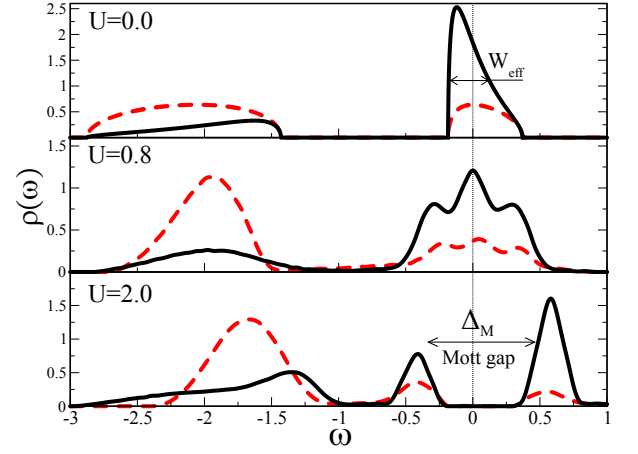


Figure 2: (Color online) Evolution of the  $f$ - (solid line) and  $p$ -orbital (dashed line) projections of the DOS. Data from QMC calculations at  $T = 0.0125$ ,  $V_{fp} = 0.9$ ,  $n_{\text{tot}} = 3$ , analytically continued on the real axis using Maximum Entropy Method<sup>41</sup>. The figure qualitatively illustrates the Mott metal-insulator transition driven by correlation in the PAM.

both in the full diagonalization and Lanczos algorithm implementations, at zero<sup>36</sup> and finite temperature.<sup>37</sup> The ED method is based on a discretization of the effective bath on an adaptive energy grid. In this paper we present full ED calculations in which the bath is described by 7 energy levels and Lanczos calculations with 8 levels. The ED calculations have been cross-checked against Density Matrix Renormalization Group, which allows to substantially increase the number of bath levels.<sup>38-40</sup>

### III. THE HOLE-DOPED MOTT INSULATOR

The PAM has been largely investigated in proximity of the Kondo insulator regime.<sup>42-44</sup> The Kondo insulator is a band insulator realized at *even* integer total filling ( $n_{\text{tot}} = 2$ ). In this regime the system has two hybridized bands with a central Kondo peak, corresponding to the resonant scattering of the conduction electrons on the localized moments and split by an indirect gap  $\Delta_{\text{ind}}$  (see fig. 1(a)). Upon doping the Kondo resonance remains pinned at the chemical potential, and the system behaves like a heavy-fermion liquid.

In this work we focus on a different model regime, namely the correlated metal obtained by a state with *odd* total occupation ( $n_{\text{tot}} = 1$  or 3) and large enough interaction. In the case of  $n_{\text{tot}} = 1$  or 3, an important role is played by the ratio  $U/\Delta$ , where  $\Delta = |\epsilon_p - \epsilon_f|$  is the charge-transfer energy, *i.e.* the separation in energy between the two electron orbitals. Two regimes can be distinguished:<sup>45</sup> (a) for  $\Delta$  smaller than  $U$  the model is in the so-called *Charge-Transfer* (CT) regime, that is expected to capture the properties of intermediate to late transition-metal oxides. Nevertheless in these systems the non-local hybridizations become important and re-

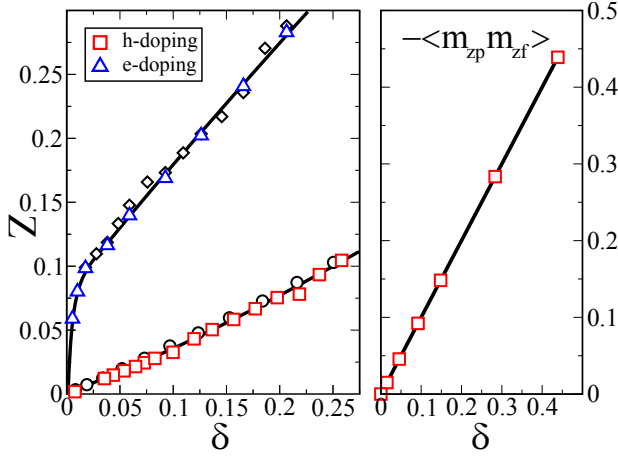


Figure 3: (Color online) Left panel: renormalization constant  $Z$  as a function of the doping  $\delta = |3 - n_{\text{tot}}|$ . Data are from Lanczos ED at  $T = 0$ ,  $U = 2$ ,  $V_{fp} = 0.9$  and increasing size of the effective bath  $N_s = 8$  (diamonds, circles) and 10 (triangles, squares). Right panel: moment-moment correlation  $-\langle m_{zp} \cdot m_{zf} \rangle$  as a function of the doping  $\delta$  in the hole doped regime. Data are from full ED calculations (see Appendix A) for  $T = 0.008$  and for the same model parameters.

quire the introduction of other terms in the Hamiltonian to be properly described. (b) For  $\Delta$  larger than  $U$  the model is in the *Mott-Hubbard* (MH) regime, which models the properties of early transition-metal oxides and heavy fermion systems, usually dominated by local physics. In this work we shall focus on this latter model regime and study the doping of a Mott insulator.

In the simplest sketch of this regime, the non-correlated band has a lower energy than the correlated one (which however is dispersive only because of the hybridization with the itinerant fermions). The latter band is in turn split by the Mott gap (see fig. 1(b)). Similarly to the Kondo Insulating regime, a heavy fermion state is obtained upon finite doping as soon as the system develops a coherent Kondo resonance signature of the insulator-metal transition.

In the following we shall briefly review the formation of a correlated metallic state by hole doping<sup>17,19</sup>. Without loss of generality, we fix the energy of the correlated orbitals at the Fermi level  $\epsilon_f = 0$  and  $\epsilon_p = -1$ , so that  $\Delta = 1$ . For  $U = V_{fp} = 0$  the model describes a system with completely filled conduction band  $n_p = 2$  and half-filled correlated orbitals with  $n_f = 1$ . For finite values of the hybridization the correlated electrons can move with an effective hopping of the order of  $t_{\text{eff}} \simeq V_{fp}^2/\Delta$ , corresponding to the indirect delocalization through the conduction band (see top panel of fig. 2). The hybridization modifies the orbitals occupation, pushing a substantial amount of the  $p$ -electron states to the Fermi level, so that  $n_p < 2$  and consequently  $n_f > 1$  and the relevant carriers are hybrid in nature. However, the  $f$ - and  $p$ -character of the model solution can still be used to indicate the projection onto the correlated and non-correlated orbital re-

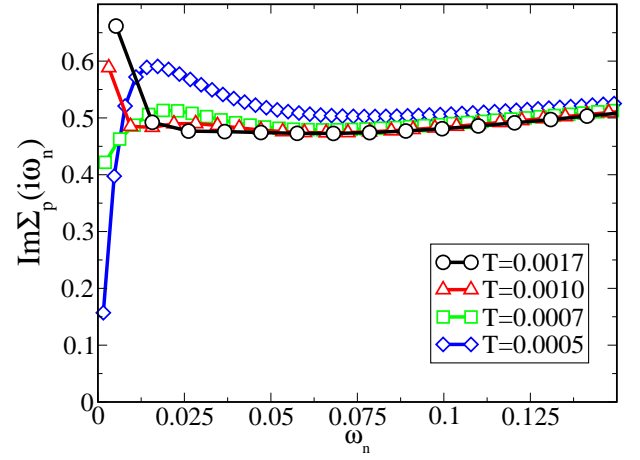


Figure 4: (Color online) Evolution of the imaginary part of the conduction electrons self-energy  $\text{Im}\Sigma_p(i\omega_n)$  for increasing temperature. Data are from finite temperature Lanczos ED with doping  $\delta = 0.1$ .

spectively. Upon increasing the interaction strength (see central panel of fig. 2) we first observe the formation of a correlated metallic state. This is characterized by the presence in the density of states (DOS) of a metallic feature at the Fermi level, flanked by the two precursors of the Hubbard bands. A Mott insulating state is then obtained further increasing the correlation  $U$ . The system opens a spectral gap at the Fermi energy (see bottom panel of fig. 2) with a width controlled by the correlation  $U$ .<sup>19</sup> To fix ideas, in the remaining part of this work we shall set the correlation and the hybridization to, respectively,  $U = 2.0$  and  $V_{fp} = 0.9$ . This choice of the model parameters corresponds to a Mott insulating state for  $n_{\text{tot}} = 3$ . Similar results can be obtained for different values of correlation and hybridization.

The Mott insulator can be destabilized in favor of a correlated metallic phase by either adding or removing electrons (creating holes). As first noticed in Ref. 17 the two transitions have a different character, ultimately related to the different role played by the non interacting band in the two cases. Doping with electrons, the extra carriers populate essentially the correlated orbitals while the  $p$ -band remains almost filled and its role is to allow the delocalization of correlated electrons. In other words, in this regime there are no multi-band effects and the hybridization plays a minor role. Therefore the  $f$ -electrons behave essentially as in a single-band Hubbard model with an effective hopping of the order of  $t_{\text{eff}}$ .

In the hole doped regime the electronic configuration is substantially different. The holes are essentially associated to the absence of  $p$ -electrons, and they tend to bind to the local moments of the almost half-filled correlated orbitals<sup>19</sup>. It is already apparent that this state can not be described by a single-band model. This effect is evident in the behavior of the inter-orbital moment-moment



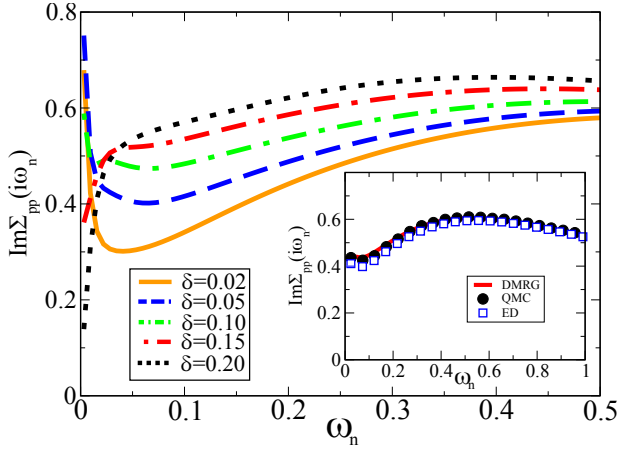


Figure 5: (Color online) Main panel: imaginary part of the conduction electrons self-energy  $\text{Im}\Sigma_p(i\omega_n)$  for increasing value of the hole doping and  $T = 0.001$ . Data are from Lanczos ED calculations. Inset: Comparison of the  $\text{Im}\Sigma_p(i\omega_n)$  behavior from different numerical methods for  $\delta = 0.05$ . The other model parameters are the same as in the main panel. The QMC and full ED calculations are performed at  $T = 0.008$ . DMRG is a  $T = 0$  calculation performed with a cluster of  $N_s = 30$  sites and plotted down to the position of the lowest energy pole.

correlation

$$\langle m_{zp} \cdot m_{zf} \rangle = \langle (n_{p\uparrow} - n_{p\downarrow}) \cdot (n_{f\uparrow} - n_{f\downarrow}) \rangle$$

reported in fig. 3, which shows how the moment of the doped p-holes aligns with the moment of the localized f-electron. The doping-driven metalization appears as the process of delocalizing a multi-band “Zhang-Rice-like” singlet state, formed by an itinerant hole bound to a localized spin, similar to that proposed in the framework of the high- $T_c$  superconductors.<sup>46</sup> The low-energy properties of this metallic state can not be straightforwardly interpreted in terms of a single-band Hubbard model,<sup>17,19</sup> and it leads to remarkable properties.

A first partial indication of the anomalous nature of this state comes from an evaluation of the quasi-particle weight  $Z = [1 - \partial \text{Im}\Sigma_f(i\omega)/\partial \omega]_{\omega \rightarrow 0}^{-1}$ , which measures the degree of metallicity of a system, being zero for a Mott insulator and one for a non-interacting metal. The results (see fig. 3) show that  $Z$  is substantially smaller for the hole-doped than for the electron-doped case, already signaling that the Zhang-Rice liquid is a poorer metal than a standard correlated metal. In the following we will show that the difference goes well beyond the quasi-particle renormalization.

#### IV. THERMAL BREAKDOWN OF THE FERMILIQUID

Fermi-liquid theory is the standard paradigm for metallic systems and describes correlated Fermi systems

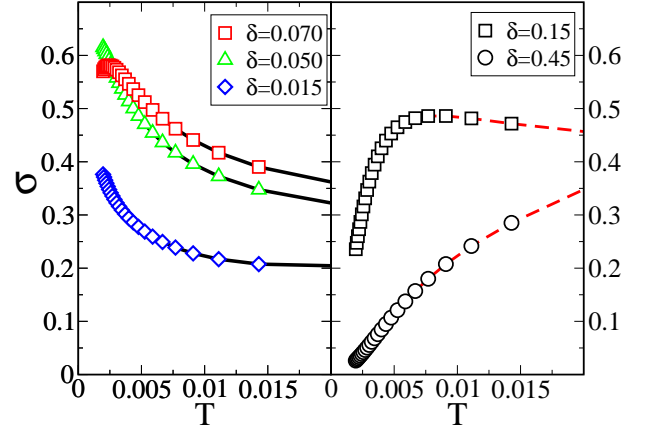


Figure 6:  $\sigma = \text{Im}\Sigma_p(i\omega_n \rightarrow 0)$  as a function of the temperature for different values of the doping. The data shown are from full ED calculations.

as a collection of non-interacting renormalized quasi-particles. DMFT studies of various correlated models have shown that even very close to the Mott transition the correlated metallic state is typically a Fermi liquid with a reduced effective hopping proportional to the quasi-particle weight  $Z$ . This scale also controls the coherence temperature above which the coherent motion of the carriers is destroyed by thermal fluctuations.

In this section we will show that the correlated metallic state of the PAM in the weakly hole-doped regime turns out to be very fragile with respect to small temperatures. More precisely, our system will be a Fermi liquid only below an extremely small coherence temperature which, for small doping, can be substantially smaller than the renormalized Fermi energy controlled by  $Z$ . Therefore the corresponding metallic state can not be described in terms of long-lived quasi-particles but is rather a liquid of short-lived singlet-like electronic excitations.

To substantiate this discussion we study the evolution of the imaginary part of the conduction electron self-energy  $\text{Im}\Sigma_p(i\omega_n)$ . The results of our calculations for  $\delta = 0.1$  are presented in fig. 4. A Fermi liquid state corresponds to a linear behavior of  $\text{Im}\Sigma_p(i\omega_n)$  at low frequency, observed only at the lowest investigated temperature,  $T = 0.0005$ . When we increase  $T$  at values of the order of  $T = 0.0007$ , two orders of magnitude smaller than the *renormalized* Fermi energy, the conduction-electron self-energy does not vanish in the  $\omega \rightarrow 0$  limit, signaling a departure from the Fermi-liquid paradigm. Further increasing the temperature leads to an enhancement of this anomaly.

In fig. 5 we follow the evolution of  $\text{Im}\Sigma_p(i\omega_n)$  for increasing doping at  $T = 0.001$ . For small doping we have a clear NFL increase at small frequency which survives up to  $\delta \simeq 0.16$ . For larger doping the system is not strongly sensitive to the Mott-Hubbard physics and the standard Fermi-liquid behavior is restored around  $\delta = 0.2$ .

The violation of the Fermi-liquid paradigm can be summarized by the temperature dependence of  $\sigma(T) =$

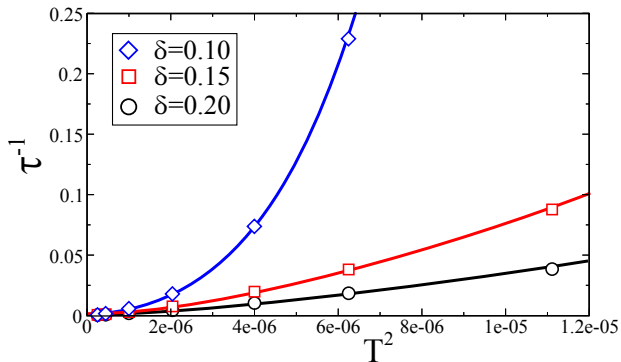


Figure 7: (Color online) Scaling of the inverse life-time  $\tau^{-1}$  as a function of  $T^2$  in the small temperature limit. Data are from Lanczos ED calculations. Lines are guide to the eye.

$\text{Im}\Sigma_p(i\omega_n \rightarrow 0)$ , reported in fig. 6. This quantity is related to the scattering rate of the carriers. In a metallic regime  $\sigma(T)$  is expected to vanish at low temperature. While for large doping (right panel)  $\sigma(T)$  vanishes as  $T \rightarrow 0$  (even if for  $\delta = 0.15$  some anomaly is observed at intermediate temperature), the small-doping data clearly confirm the NFL behavior down to very small temperature, even if, strictly at  $T = 0$  the vanishing  $\sigma$  would be recovered.

Finally, fig. 7 depicts the inverse life-time  $\tau^{-1} = Z_p \sigma$  of the doped carriers, where  $Z_p^{-1} = 1 - \text{Im}\Sigma_p(i\omega_1)/\pi T$ . In a Fermi liquid  $\tau^{-1}$  grows as  $T^2 \sim \omega^2$  at low temperature. Our calculations for small doping show a decay faster than  $T^2$  which strengthens the picture of an incoherent metallic state. Once again, a Fermi-liquid behavior is established only at extremely low temperatures if the doping is small, while the large-doping data recover the standard behavior.

The increasing scattering rate as a function of decreasing temperature is usually associated to scattering with impurities<sup>14</sup>. In this spirit, in the following we will interpret our results as the scattering of the carriers with fluctuating local moments. This effect can be understood as the results of the competition between the aforementioned tendency to form local Zhang-Rice-singlets, driven by the hole-doping, and the incoherent nature of the scatterer provided by the  $f$ -electron local moments, driven by Mott physics. At large doping the increased number of available holes of  $p$ -type helps the formation of a many-body coherent state without breaking the local binding with  $f$ -moment. This arguments will be substantiated by the calculations that we report in the following sections.

### A. The coherence temperature

The analysis of the self-energy and of the carriers lifetime clearly shows the existence of a small doping-dependent energy scale associated with the appearance of an incoherent metal. We expect this scale to influence

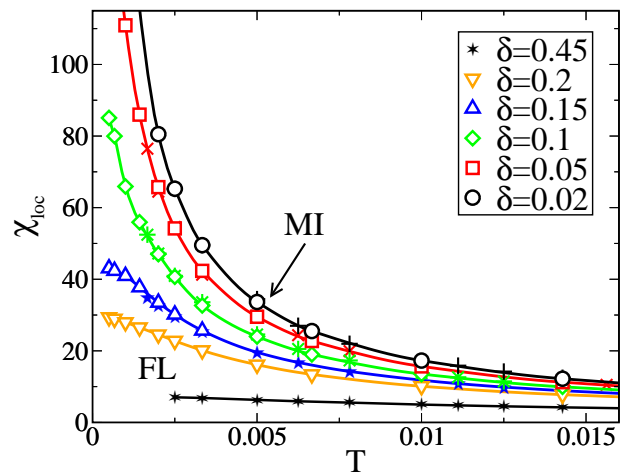


Figure 8: (Color online) Local spin susceptibility  $\chi_{\text{loc}}$  as a function of the temperature and increasing value of the hole doping. Data are from Lanczos ED (open symbols) and full ED (pluses, crosses and stars symbols) calculations.

also other observables, like the local spin susceptibility:

$$\chi_{\text{loc}}(T) = \int_0^\beta \langle S_{zf}(\tau) \cdot S_{zf}(0) \rangle d\tau$$

This quantity describes the response to a *local* magnetic field and easily discriminates between a Fermi-liquid, in which the zero-temperature limit is a constant (Pauli susceptibility), and a paramagnetic Mott insulator in which it diverges like  $1/T$  (Curie behavior).

The results are reported in fig. 8. In the Mott insulating state ( $\delta = 0$ ) the magnetic moments of the localized  $f$ -electrons essentially behave as free spins, we thus obtain the typical Curie behavior with a  $1/T$  dependence for the spin susceptibility. The slightly hole-doped regime does not show the behavior of a standard metal, namely  $\chi_{\text{loc}}$  keeps on increasing down to the lowest investigated temperature  $T \simeq 10^{-3}D$  without any sign of saturation. The enhancement of the spin susceptibility signals the presence of unquenched local moments and can be associated to protracted screening effect.<sup>47</sup> Only for larger doping, the susceptibility saturates to large constant value at very low temperature.

The presence of enhanced low- $T$  spin susceptibility coexisting with a (bad) metallic behavior substantiates the idea that the hole-doped system can be regarded as formed by nearly free (incoherent) moments, and an underlying metallic host formed by the doped holes which are prevented from coherently delocalize by local coupling to  $f$ -moments. This interpretation leads us to estimate the coherence temperature  $T_{\text{coh}}$  from

$$\chi_{\text{loc}}^{-1}(T) \propto T + T_{\text{coh}} \quad (8)$$

We plot the resulting values, obtained with different numerical methods, in fig. 9. In the same plot we report the crossover points estimated from the temperature evolution of the imaginary part of the self-energy

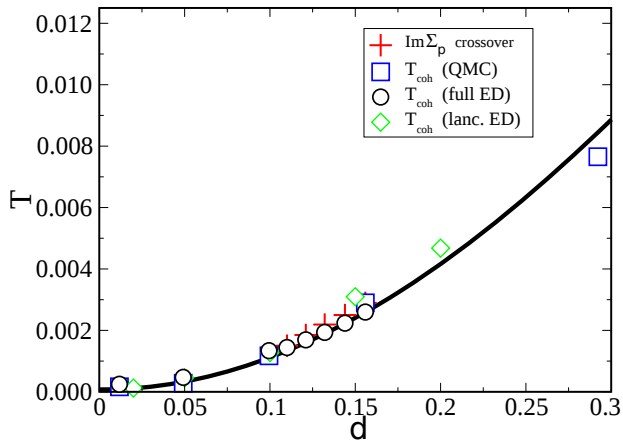


Figure 9: (Color online) Coherence temperature scale  $T_{\text{coh}}$  as extrapolated from the inverse local spin susceptibility  $\chi_{\text{loc}}^{-1}(T)$ . The extrapolations from different numerical methods are found to be in satisfactory agreement.

$\Sigma_p$  (red crosses). The good agreement of these points with the extrapolated data validates the physical interpretation of the coherence temperature. It is unfortunately very hard to identify the functional form of the coherence temperature due to the smallness of the scale involved and the numerical uncertainties. However, the data are compatible with an exponential behavior of the form  $T_{\text{coh}} \simeq B e^{-A/\delta}$ , which has been obtained within the  $1/N$  approximation in the infinite- $U$  Kondo limit<sup>48</sup>.

The phase diagram in the doping-temperature plane, presented in fig. 10, can help us to summarize the scenario emerging from our calculations. The diagram reveals the character of the DMFT solution in proximity of the Mott insulating state through the behavior of the  $\text{Im}\Sigma_p(i\omega_n \rightarrow 0)$ . Using finite temperature Lanczos ED method we investigated a smaller temperature scale with respect to that studied in Ref. 18. A large value of the  $\text{Im}\Sigma_p(i\omega_n \rightarrow 0)$  testifies a NFL behavior and the results clearly show that the highly incoherent state emerges from the Mott state and occupies a sizable region of the phase diagram. The NFL region is separated from the coherent metal by a crossover taking place at  $T_{\text{coh}}$  defined above, which therefore confirms its meaning as the temperature in which the metal loses coherence.

## V. MAGNETIC PROPERTIES

### A. External magnetic field

We have shown that hole-doping the Mott insulating phase of the periodic Anderson model leads to peculiar charge carriers, so that the motion of the created  $p$ -holes occurs through the formation of Zhang-Rice singlets, in which the spins of the conduction electrons are anti-ferromagnetically correlated with the localized spins. As a consequence, we expect that a magnetic field can have

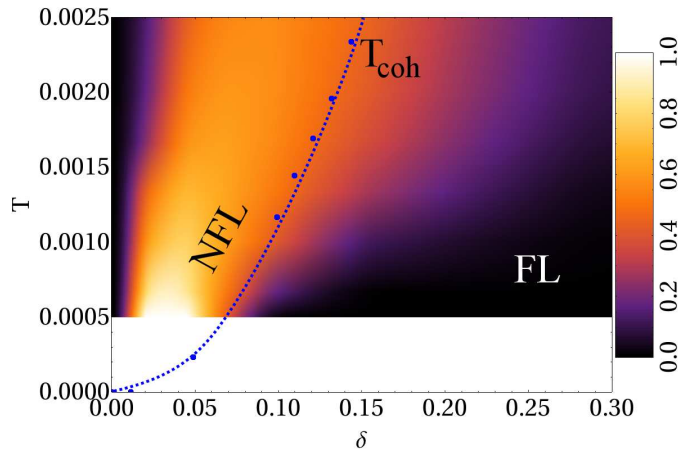


Figure 10: (Color online) Phase-diagram of the PAM near the Mott insulating state as a function of temperature and hole-doping. The diagram is obtained from  $\text{Im}\Sigma_p(i\omega_n \rightarrow 0)$ . The dotted line indicates the crossover temperature scale  $T_{\text{coh}}$ .

important and surprising effects on this phase, showing a further difference with respect to a standard Fermi liquid.

In the model regime investigated in this work, the main source of magnetism comes from the  $f$ -electrons. The conduction band is almost completely filled, so that the magnetization of the few singly occupied orbitals, favored by hole doping, is not expected to contribute significantly to the magnetic properties of the system.

Nevertheless, conduction band electrons can be indirectly affected by the magnetic polarization of the  $f$ -orbital moments, through their local binding. To illustrate this point, we show in fig. 11 the evolution of the low energy part of  $\text{Im}\Sigma_p(i\omega_n)$  as a function of a uniform magnetic field  $\mathbf{B}$ . Apparently the NFL state turns into a normal metallic state by the action of an external magnetic field. It is however worth noting that the Fermi liquid is recovered for  $B \simeq 0.05D$ , a huge value if compared with experimentally accessible fields. This large value is a direct consequence of the large (order one) value of  $V_{fp}$ , chosen to emphasize the hybridization effects and their role in the conduction properties of the model. Smaller and more realistic values of this parameter are expected to reduce the critical field by reducing the charge fluctuations at correlated  $f$ -orbitals.

The crossover to a Fermi liquid state driven by external magnetic field is not surprising in light of our analysis. Upon increasing the magnetic field a larger and larger number of local  $f$ -moments are polarized. When the moments are aligned, the  $p$ -holes can move essentially freely in the ferromagnetic background without breaking the singlet state with the localized spins. Therefore the source of scattering disappears and the metallic state recovers the Fermi-liquid coherence. In other words the polarization of  $f$ -orbital local moments allows the conduction electron cloud to dynamically screen the correlated electrons local moments, dramatically increasing the coherence scale of the system.

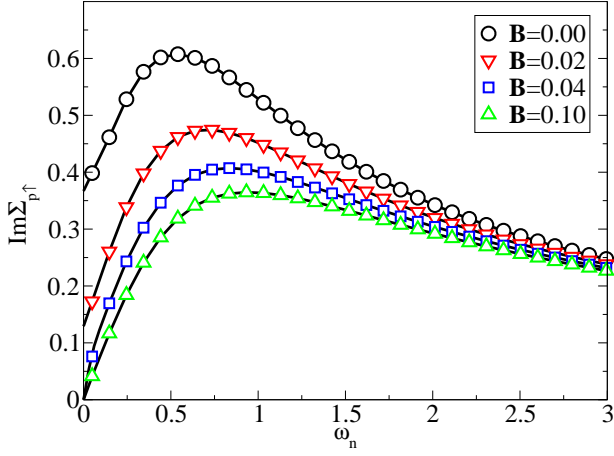


Figure 11: (Color online) Imaginary part of the majority-spin  $p$ -electron self-energy for increasing external magnetic field  $\mathbf{B}$ . The data are from QMC solution at  $T = 0.016$  and  $\delta = 0.05$ .

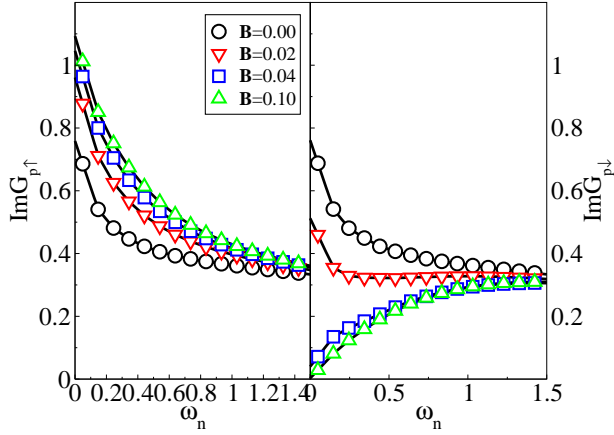


Figure 12: Imaginary part of conduction band electron Green's function  $\text{Im}G_{p\sigma}(i\omega_n)$  for  $T = 0.016$ ,  $\delta = 0.05$  and increasing strength of external magnetic field. Data from QMC calculations.

The coherent motion of the doped carriers with the opposite spin of the localized momenta (majority spin) should then be balanced by the insulating nature of the minority spins carriers. This effect is illustrated in the fig. 12. In this figure we show the behavior of both spin species conduction electrons Green's function for the same strengths of the external magnetic field as used in fig. 11. Left panel shows the increasing metalization of the majority spin charge carriers, whereas in the right panel we show how minority spins are driven towards an insulating state by increasing magnetic field.

### B. Anti-ferromagnetic ordering

At low temperature, we expect the development of anti-ferromagnetic (AFM) correlations a result of super-exchange between neighboring  $f$ -electrons assisted by the

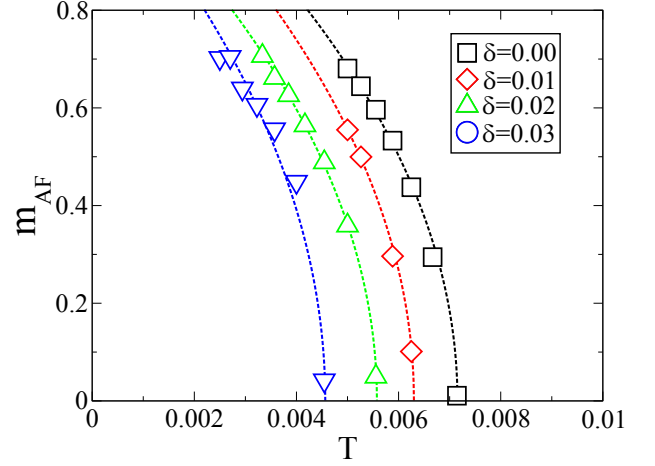


Figure 13: (Color online) Main panel: Staggered magnetization  $m_{AF}$  as a function of temperature and increasing value of hole-doping. The data are from full ED calculations.

hybridization with  $p$ -orbital states. In this section we investigate the onset of an AFM long-range ordered state and its effect on the coherence scale using the extension of the DMFT equations to long-range order detailed in Appendix B.

To begin with we report in fig. 13 the staggered magnetization  $m_{AF} = 1/N \sum_i (-1)^i \langle n_{fi\uparrow} - n_{fi\downarrow} \rangle$  as a function of the temperature for various doping. The transition appears to be of second order in the whole doping region. The Néel temperature  $T_N$ , extracted from a power-law fit of the data, is maximum at zero doping and decreases by adding holes, as in the single-band Hubbard model.<sup>53</sup>

The onset of an AFM ordering of the local  $f$ -moments reinstates the Fermi liquid properties in the tiny hole-doped regime. This effect is illustrated in the left panel of fig. 14, where we present the evolution of the imaginary part of  $\Sigma_{p\sigma}(i\omega_n)$  from the paramagnetic NFL phase to the AFM ordered phase. The large finite intercept present in NFL phase is driven to zero in the AFM ordered phase. Nevertheless, the metallic character of the solution is preserved across the transition, as illustrated in the right panel of the same figure by comparing the imaginary parts of the conduction electrons Green's functions in the two phases. The ordering of the local moments in a Néel state, allows the doped charge carriers to form coherent electronic waves (with doubled wave-vector) and to get delocalized. However, as mentioned above, the AFM state is only stable in a small window of doping and the NFL remains stable for a wide range of parameters.

### C. Magnetic stability

The common wisdom about systems of concentrated impurities described by the PAM is that long-range magnetic ordering is likely to set in, especially if the metallic



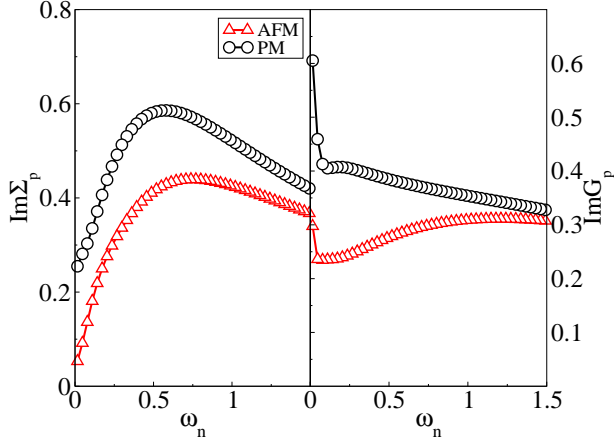


Figure 14: (Color online) Conduction electrons self-energy  $\text{Im}\Sigma_p(i\omega_n)$  (left panel) and Green's function  $\text{Im}G_p(i\omega_n)$  (right panel). Data from full ED calculations for  $\delta = 0.01$  and  $T = 0.005$ .

state is weakened by correlations as in our case.

Our results for the AFM state suggest instead a remarkable stability of the incoherent metallic state as the long-range order is confined to low temperature and small doping concentration. In this section we discuss the physical origin of this surprising result.

At small doping near the Mott insulating state neighboring  $f$ -orbital electrons develop AFM correlations as a results of super-exchange. These processes are of the fourth order in the hybridization with a leading energy scale of the order:<sup>43</sup>  $J_{SE} \propto W_{\text{eff}}^2/U \sim V_{fp}^4/\Delta^2 U$

On the other hand it is easy to realize that at large doping *ferromagnetic* correlations are expected because of the fact that the doped carriers are locked in singlets with the localized  $f$ -spins. In an AFM or disordered background, the motion of the  $p$ -holes requires to break the singlet and it is therefore strongly inhibited, leading to the lack of coherence that we discussed at length. Moreover it leaves a local moment unscreened, increasing the fluctuations in the local magnetization. Conversely, a ferromagnetic alignment of the localized spins allows for an unperturbed delocalization of the carriers, with a mechanism which is closely reminiscent of the double-exchange,<sup>49–51</sup> where the coupling between conduction electrons and localized spins is given by the ferromagnetic Hund's coupling.

Therefore, upon increasing the doping the tendency to form AFM ordering is contrasted by the increased relevance of the kinetic energy and eventually it becomes more favorable to sacrifice the gain in super-exchange energy in order to gain the kinetic energy associated to the ferromagnetic background. This leads, most importantly, to an intermediate region between the two regimes in which the local magnetization is strongly fluctuating.

From this discussion it is natural to associate the fluctuations of the local magnetization to the scattering mechanism that leads to the poor coherence. To test this

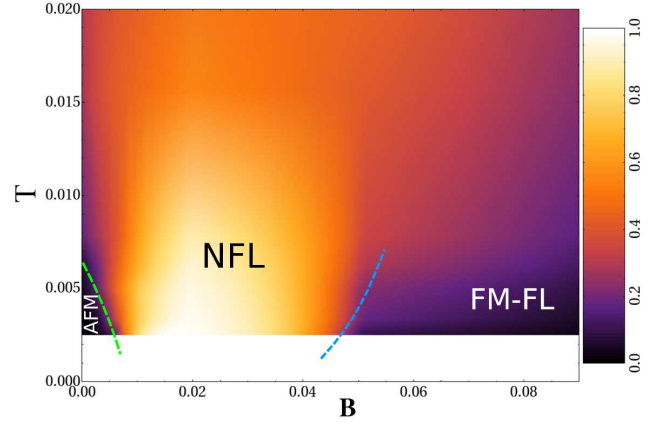


Figure 15: (Color online) Intensity plot of  $\text{Im}\Sigma_p(\omega \rightarrow 0)$  as a function of external magnetic field  $\mathbf{B}$  and  $T$  at fixed doping  $\delta = 0.01$ . For visualization, the data have been normalized to  $\max\{\text{Im}\Sigma_p(\omega_n)\}$  at each  $(\mathbf{B}, T)$ . Dashed lines are drawn to better visualize the crossover regions in the phase-diagram.

idea we study the response of the system in the AFM ordered metallic phase to the application of a uniform magnetic field  $\mathbf{B}$  which will clearly favor the ferromagnetic tendency.

The results are summarized in the phase diagram of fig. 15, determined again using  $\text{Im}\Sigma_p(i\omega_n \rightarrow 0)$ . Details of the calculations are given in Appendix B. Doping is fixed to  $\delta = 0.01$ , safely into the AFM ordered region in the limit  $\mathbf{B} \rightarrow 0$ .

The phase-diagram shows that the AFM order survives the effects of the external magnetic field up to small strengths ( $B \simeq 0.01$ ). In this region the solution keeps the coherent metallic character enforced by the long-range magnetic ordering. Nevertheless, for larger values of the magnetic field the system is driven to an incoherent state with finite-temperature NFL behavior, as indicated by the increased scattering (light color). In this regime the large applied field tends to magnetically polarize the AFM ordered  $f$ -moments, producing their strong frustration and ultimately leading to the formation of an incoherent magnetic background for the motion of the doped carriers. Further increasing the strength of the magnetic field triggers the formation of a ferromagnetic ordering of the  $f$ -moments and a fully polarized (coherent) metallic state (right dark coloured area).

The most striking observation is that the present diagram faithfully mirrors the diagram as a function of doping, clearly suggesting that the evolution of the conduction properties as a function of doping is associated to the transition from the AFM state to the ferromagnetic regime and that the poorly coherent metal establishes precisely in the intermediate region, dominated by the local spin fluctuations which appear as the source of the scattering mechanism which opposes to the coherent motion of the holes.

## VI. CONCLUSIONS AND PERSPECTIVES

In this work we presented a detailed dynamical mean-field theory study of the properties of the unconventional metallic state obtained by doping with holes the Mott insulator in the periodic Anderson model. We discuss in details the non-Fermi liquid behavior of the system and the mechanism that is behind the suppression of the coherence scale.

In this regime the holes have mainly  $p$ -character, but they tend to bind to the correlated  $f$ -electrons to form a Zhang-Rice-like singlet state. The formation of this composite object leads to a highly incoherent metallic state which deviates from a standard Fermi-liquid above a coherence temperature which decreases very rapidly upon reducing doping, and it is much smaller than the effective Fermi energy that one could estimate from the degree of correlation of the system, *i.e.*  $T_{\text{coh}} \ll ZD$ .

We characterize this anomalous behavior by studying the scattering properties of the carriers and by computing the inverse lifetime and local spin susceptibility, which allow us to quantitatively estimate the coherence temperature characterizing the breakdown of the standard Fermi liquid and to describe the onset of an incoherent metal with finite lifetime.

The highly incoherent metal is unstable towards antiferromagnetic ordering only at very small doping, while at large doping ferromagnetic correlations develop and favour a regular metallic behavior supported by a mechanism which reminds the double-exchange physics. The intermediate region, where the motion of the holes is not coherent, is therefore dominated by large fluctuations of the  $f$ -spins, which provide the scattering channel responsible of the finite lifetime of the carriers.

The relation between magnetic fluctuations and the breakdown of the standard FL scenario is emphasized by observing that an external uniform magnetic field, which obviously destroys AFM ordering favoring a ferromagnetic alignment, mirrors the effect of doping and leads again to a wide region of high incoherence between the two magnetically ordered states.

We emphasize that the path to poor coherence discussed in this paper only depends on two general features of strongly correlated materials, namely the Mott physics which leads to the localization of carriers and multi-orbital physics necessary to the local singlet formation. In this light, we expect that the mechanism outlined here can be a rather general source of violation of Fermi liquid paradigm and incoherent behavior, and it can be relevant for example to heavy fermions, but also, with some important differences related to the  $d$ -wave symmetry of the Zhang-Rice singlets, to the cuprate superconductors.

Finally, a natural question to address is to what extent our findings can be considered the local portrait of the presence of a quantum critical point, hidden by the absence of spatial fluctuations. Indeed, the existence of a quantum critical point in the PAM, although in a differ-

ent model regime, has already been pointed in Ref. 52, using cluster extension of the DMFT. The development of our work along this direction, in order to clarify the fate of the small coherence scale in presence of short-range spatial fluctuations, is left for future research.

## Acknowledgments

A.A., G.S. and M.R. thank M. Gabay, D.J. Garcia, E. Miranda for the many useful discussions and suggestions. A.A. is also grateful to V. Dobrosavljević. A.A. acknowledges support from the ESRT Marie-Curie program during part of this work. L.d.M. acknowledges support from the Agence Nationale de la Recherche (ANR-09-RPDOC-019-01) and the RTRA “Triangle de la Physique”. A.A. and M.C. are financed by European Research Council under FP7/ERC Starting Independent Research Grant “SUPERBAD” (Grant Agreement n. 240524)

## Appendix A: Two-orbital effective impurity model

The calculation of physical quantities internal to the local “ $pf$ -dimer”, such as the moment-moment correlation function  $\langle m_{zp} \cdot m_{zf} \rangle$  can be performed within single-site DMFT using an alternative formulation of the effective impurity problem in which the local  $p$ -orbital is not integrated out in the construction of the effective action. Thus the original lattice system is reduced to the problem of a single dimer embedded in an electronic bath. The corresponding effective action has a  $2 \times 2$  matrix structure in the orbital space and reads:

$$\begin{aligned} \hat{S}'_{\text{eff}} = & - \int_0^\beta d\tau \int_0^\beta d\tau' \sum_\sigma \psi_{0\sigma}^+(\tau) \hat{\mathcal{G}}_0^{-1}(\tau - \tau') \psi_{0\sigma}(\tau') \\ & + U \int_0^\beta d\tau [n_{f0\uparrow}(\tau) - 1/2][n_{f0\downarrow}(\tau) - 1/2] \end{aligned}$$

The Weiss Field  $\hat{\mathcal{G}}_0^{-1}(i\omega_n)$  describes the local quantum fluctuations at the tagged dimer. The Bethe lattice self-consistency becomes

$$\hat{\mathcal{G}}_0^{-1}(i\omega_n) = \begin{pmatrix} i\omega_n + \mu - \epsilon_p - \frac{D^2}{4} G_p(i\omega_n) & -V_{fp} \\ -V_{fp} & i\omega_n + \mu - \epsilon_f \end{pmatrix}$$

The DMFT algorithm for the two-orbital representation proceeds as in the standard case. The effective two-orbital impurity problem is solved to determine the impurity Green’s functions:

$$G_\alpha^{imp}(i\omega_n) = -i \langle \alpha \alpha^+ \rangle_{\hat{S}'_{\text{eff}}}$$

with  $\alpha = p, f$ . Next, the conduction electron self-energy  $\Sigma_p$  can be determined using the Dyson equation and used to evaluate the local Green’s function  $G_p$  which is necessary to update the local Weiss field. The whole algorithm is iterated until convergence is reached.

## Appendix B: Long range order

The DMFT equations can be extended to describe phases with long range magnetic ordering<sup>16</sup>. Here we derive the equations for the anti-ferromagnetic order in the two-orbital effective problem, considering also the effect of a uniform magnetic field. Similar equations can be derived for the single-orbital effective model.

On a bipartite lattice crystal as our Bethe lattice, we can define two sub-lattices  $A$  and  $B$ , such that nearest-neighbor hopping always connects one  $A$ -site with a  $B$ -site. Then we can introduce a four-component spinor with orbital and sub-lattice indices so that the bare lattice propagator takes the form:

$$\hat{G}_{0\mathbf{k}\sigma}^{-1} = \begin{pmatrix} \alpha_A & -\epsilon(\mathbf{k}) & -V_{fp} & 0 \\ -\epsilon(\mathbf{k}) & \alpha_B & 0 & -V_{fp} \\ -V_{fp} & 0 & i\omega_n - \epsilon_f + \mu_A & 0 \\ 0 & -V_{fp} & 0 & i\omega_n - \epsilon_f + \mu_B \end{pmatrix}$$

with  $\alpha_s = i\omega_n - \epsilon_p + \mu_s$  and  $s = A, B$ . The corresponding Green's functions are obtained via the Dyson equation with the diagonal self-energy matrix with components  $\{0, 0, \Sigma_{A\sigma}, \Sigma_{B\sigma}\}$ . The  $p$ -electrons local Green's functions, required to close the DMFT equations, now read:

$$G_{pA\sigma}(\mathbf{k}, i\omega_n) = \sum_{\mathbf{k}} \frac{\zeta_{B\sigma}}{\zeta_{A\sigma}\zeta_{B\sigma} - \epsilon(\mathbf{k})^2}$$

where:

$$\begin{aligned} \zeta_{s\sigma} &= \alpha_s - \frac{V_{fp}^2}{\gamma_{s\sigma}} \\ \gamma_{s\sigma} &= i\omega_n - \epsilon_f + \mu_s - \Sigma_{s\sigma}(i\omega_n) \end{aligned}$$

In the case of anti-ferromagnetic ordering it is not necessary to take explicitly into account both sublattices. Observing that:

$$\Sigma_{A\sigma}(i\omega_n) = \Sigma_{B-\sigma}(i\omega_n) = \Sigma_{\sigma}(i\omega_n)$$

and thus:

$$\zeta_{A\sigma} = \zeta_{B-\sigma} = \zeta_{\sigma} \quad (\text{B1})$$

we can eliminate one of the two sublattices and recover a  $2 \times 2$  formalism with a Weiss field given by

$$\hat{G}_{0\sigma}^{-1}(i\omega_n) = \begin{pmatrix} \alpha_{\sigma} - \frac{D^2}{4} G_{p-\sigma}(i\omega_n) & -V_{fp} \\ -V_{fp} & i\omega_n + \mu_{\sigma} - \epsilon_f \end{pmatrix}$$

The local conduction electron Green's function  $G_{p\sigma}(i\omega_n)$  can be expressed in terms of the following Hilbert transform:

$$G_{p\sigma}(i\omega_n) = \zeta_{-\sigma} \int_{\mathbb{R}} d\varepsilon \frac{\rho_0(\varepsilon)}{\zeta_{\sigma}\zeta_{-\sigma} - \varepsilon^2}$$

which closes the set of DMFT equations.

In presence of a uniform magnetic field  $\mathbf{B}$  in the ordered phase of the system, the symmetry relation Eq. (B1) between the two sublattices does not hold. Therefore the DMFT solution requires to explicitly consider the two sublattices and the self-consistency equations for the four components of the Weiss field  $\mathcal{G}_{0s\sigma}(i\omega_n)$  ( $s = A, B$  and  $\bar{s} = B, A$ ) read

$$\mathcal{G}_{0s\sigma}^{-1} = i\omega_n + \bar{\mu}_{s\sigma} - \epsilon_f - \frac{V_{fp}^2}{i\omega_n + \bar{\mu}_{s\sigma} - \epsilon_p - \frac{D^2}{4} G_{p\sigma\bar{s}}(i\omega_n)}$$

where the coupling to the magnetic field  $\mathbf{B}$  has been included in a redefinition of the chemical potential  $\bar{\mu}_{s\sigma} = \mu_{s\sigma} + \sigma\mathbf{B}/2$ . This means that at each iteration we need to solve two impurity models, one for each sub-lattice and that the solution of one sub-lattice will determine the Weiss field for the other.

- 
- <sup>1</sup> N. Ashcroft and N. Mermin, *Solid State Physics* (Saunders College, Philadelphia, 1976).
  - <sup>2</sup> M. Imada, A. Fujimori, and Y. Tokura, *Rev. Mod. Phys.* **70**, 1039 (1998).
  - <sup>3</sup> N. F. Mott, *Metal-insulator transitions* (Taylor & Francis, London, 1974).
  - <sup>4</sup> J. G. Bednorz and K. A. Müller, *Zeit. Phys. B* **64**, 189 (1986).
  - <sup>5</sup> P. W. Anderson, *Science* **235**, 1196 (1987).
  - <sup>6</sup> J. Flouquet, G. Knebel, D. Braithwaite, D. Aoki, J.-P. Brison, F. Hardy, A. Huxley, S. Raymond, B. Salce, and I. Sheikin, *Comptes Rendus Physique* **7**, 22 (2006).
  - <sup>7</sup> N. Mathur, F. Grosche, S. Julian, I. Walker, D. Freye, R. Haselwimmer, and G. Lonzarich, *Nature* **394**, 39 (1998).
  - <sup>8</sup> Y. Kamihara, T. Watanabe, M. Hirano, and H. Hosono, *J. Am. Chem. Soc.* **130**, 3296 (2008).

- <sup>9</sup> Y. Takabayashi, A. Y. Ganin, P. Jeglič, D. Arčon, T. Takano, Y. Iwasa, Y. Ohishi, M. Takata, N. Takeshita, K. Prassides, et al., *Science* **323**, 1585 (2009).
- <sup>10</sup> M. Capone, M. Fabrizio, C. Castellani, and E. Tosatti, *Rev. Mod. Phys.* **81**, 943 (2009).
- <sup>11</sup> R. Mitsuhashi, Y. Suzuki, Y. Yamanari, H. Mitamura, T. Kambe, N. Ikeda, H. Okamoto, A. Fujiwara, M. Yamaji, N. Kawasaki, et al., *nature* **464**, 76 (2010).
- <sup>12</sup> G. Giovannetti and M. Capone, *Phys. Rev. B* **83**, 134508 (2011).
- <sup>13</sup> Y. Nomura, K. Nakamura, and R. Arita, *cond-mat/1112.3483* (2011).
- <sup>14</sup> G. R. Stewart, *Rev. Mod. Phys.* **73**, 797 (2001).
- <sup>15</sup> P. Nozières, *Theory of Interacting Fermi systems* (West-

- view Press, 1997).
- <sup>16</sup> A. Georges, G. Kotliar, W. Krauth, and M. J. Rozenberg, *Rev. Mod. Phys.* **68**, 13 (1996).
  - <sup>17</sup> G. Sordi, A. Amaricci, and M. J. Rozenberg, *Phys. Rev. Lett.* **99**, 196403 (2007).
  - <sup>18</sup> A. Amaricci, G. Sordi, and M. J. Rozenberg, *Phys. Rev. Lett.* **101**, 146403 (2008).
  - <sup>19</sup> G. Sordi, A. Amaricci, and M. J. Rozenberg, *Phys. Rev. B* **80**, 035129 (2009).
  - <sup>20</sup> N. Grewe, T. Pruschke, and H. Keiter, *Zeit. Phys. B* **71**, 75 (1988).
  - <sup>21</sup> D. M. Newns and N. Read, *Adv. in Phys.* **36** (1987).
  - <sup>22</sup> H. Schweitzer and G. Czycholl, *Phys. Rev. Lett.* **67**, 3724 (1991).
  - <sup>23</sup> P. Fazekas and B. H. Brandow, *Phys. Scr.* **36** (1987).
  - <sup>24</sup> T. Pruschke, R. Bulla, and M. Jarrell, *Phys. Rev. B* **61**, 12799 (2000).
  - <sup>25</sup> C. Noce, *Phys. Rep.* **431**, 173 (2006).
  - <sup>26</sup> P. Gurin and Z. Gulácsi, *Phys. Rev. B* **64**, 045118 (2001).
  - <sup>27</sup> Z. Gulácsi, *Eur. Phys. J. B* **30**, 295 (2002).
  - <sup>28</sup> H. Shiba and P. Fazekas, *Prog. Theor. Phys.* **101**, 403 (1990).
  - <sup>29</sup> M. Jarrell, *Phys. Rev. B* **51**, 7429 (1995).
  - <sup>30</sup> M. J. Rozenberg, *Phys. Rev. B* **52**, 7369 (1995).
  - <sup>31</sup> G. Kotliar and D. Vollhardt, *Phys. Today* **57**, 53 (2004).
  - <sup>32</sup> W. Metzner and D. Vollhardt, *Phys. Rev. Lett.* **62**, 324 (1989).
  - <sup>33</sup> P. Coleman, *Heavy Fermions: Electrons at the Edge of Magnetism*, Handbook of Magnetism and Advanced Magnetic Materials (John Wiley & Sons, Ltd, 2007).
  - <sup>34</sup> G. Kotliar, S. Y. Savrasov, K. Haule, V. S. Oudovenko, O. Parcollet, and C. A. Marianetti, *Rev. Mod. Phys.* **78**, 865 (2006).
  - <sup>35</sup> R. R. dos Santos, *Br. J. Phys.* **33**, 36 (2003).
  - <sup>36</sup> E. Dagotto, *Rev. Mod. Phys.* **66**, 763 (1994).
  - <sup>37</sup> M. Capone, L. de' Medici, and A. Georges, *Phys. Rev. B* **76**, 245116 (2007).
  - <sup>38</sup> U. Schollwöck, *Rev. Mod. Phys.* **77**, 259 (2005).
  - <sup>39</sup> K. A. Hallberg, *Phys. Rev. B* **52**, R9827 (1995).
  - <sup>40</sup> D. J. García, K. Hallberg, and M. J. Rozenberg, *Phys. Rev. Lett.* **93**, 246403 (2004).
  - <sup>41</sup> J. E. Gubernatis, M. Jarrell, R. N. Silver, and D. S. Sivia, *Phys. Rev. B* **44**, 6011 (1991).
  - <sup>42</sup> J. R. Schrieffer and P. A. Wolff, *Phys. Rev.* **149**, 491 (1966).
  - <sup>43</sup> P. Fazekas, *Lecture Notes on Electron Correlation and Magnetism* (Singapore: World Scientific, 1999).
  - <sup>44</sup> S. Doniach, *Physica B* **91**, 231 (1977).
  - <sup>45</sup> J. Zaanen, G. A. Sawatzky, and J. W. Allen, *Phys. Rev. Lett.* **55**, 418 (1985).
  - <sup>46</sup> F. C. Zhang and T. M. Rice, *Phys. Rev. B* **37**, 3759 (1988).
  - <sup>47</sup> A. N. Tahvildar-Zadeh, M. Jarrell, and J. K. Freericks, *Phys. Rev. B* **55**, R3332 (1997).
  - <sup>48</sup> S. Burdin, A. Georges, and D. R. Grempel, *Phys. Rev. Lett.* **85**, 1048 (2000).
  - <sup>49</sup> C. Zener, *Phys. Rev.* **82**, 403 (1951).
  - <sup>50</sup> P. W. Anderson and H. Hasegawa, *Phys. Rev.* **100**, 675 (1955).
  - <sup>51</sup> P. G. de Gennes, *Phys. Rev.* **118**, 141 (1960).
  - <sup>52</sup> L. De Leo, M. Civelli, and G. Kotliar, *Phys. Rev. B* **77**, 075107 (2008).
  - <sup>53</sup> The nature of the transition makes the precise determination of the doping value at which the ordering temperature vanishes numerically hard. Nevertheless, the data available at smaller doping concentrations suggest the AFM region to be bounded by  $\delta = 0.1$  at zero temperature